Cell

Store-Independent Activation of Orai1 by SPCA2 in Mammary Tumors

Mingye Feng,[1] Desma M. Grice,[3,6] Helen M. Faddy,[3,6] Nguyen Nguyen,[2,6] Sharon Leitch,[1] Yingyu Wang,[5] Sabina Muend,[1] Paraic A. Kenny,[4] Saraswati Sukumar,[2] Sarah J. Roberts-Thomson,[3] Gregory R. Monteith,[3] and Rajini Rao[1,*]
[1]Department of Physiology
[2]Department of Oncology
School of Medicine, The Johns Hopkins University, Baltimore, MD 21205, USA
[3]School of Pharmacy, The University of Queensland, Brisbane, QLD 4072, Australia
[4]Department of Developmental and Molecular Biology, Albert Einstein Cancer Center, Albert Einstein College of Medicine, Bronx, NY 10461, USA
[5]Department of Mechanical Engineering, Whiting School of Engineering, The Johns Hopkins University, Baltimore, MD 21218, USA
[6]These authors contributed equally to this work
*Correspondence: rrao@jhmi.edu
DOI 10.1016/j.cell.2010.08.040

SUMMARY

Ca^{2+} is an essential and ubiquitous second messenger. Changes in cytosolic Ca^{2+} trigger events critical for tumorigenesis, such as cellular motility, proliferation, and apoptosis. We show that an isoform of Secretory Pathway Ca^{2+}-ATPase, SPCA2, is upregulated in breast cancer-derived cells and human breast tumors, and suppression of SPCA2 attenuates basal Ca^{2+} levels and tumorigenicity. Contrary to its conventional role in Golgi Ca^{2+} sequestration, expression of SPCA2 increased Ca^{2+} influx by a mechanism dependent on the store-operated Ca^{2+} channel Orai1. Unexpectedly, SPCA2-Orai1 signaling was independent of ER Ca^{2+} stores or STIM1 and STIM2 sensors and uncoupled from Ca^{2+}-ATPase activity of SPCA2. Binding of the SPCA2 amino terminus to Orai1 enabled access of its carboxyl terminus to Orai1 and activation of Ca^{2+} influx. Our findings reveal a signaling pathway in which the Orai1-SPCA2 complex elicits constitutive store-independent Ca^{2+} signaling that promotes tumorigenesis.

INTRODUCTION

Basal Ca^{2+} concentrations are tightly controlled within a narrow submicromolar range by an array of Ca^{2+} channels and pumps that are susceptible to dysregulation in cancer. Transient changes in cytosolic Ca^{2+} induce downstream signaling events, which regulate a wide range of cellular functions (Berridge et al., 2003; Clapham, 2007; Roderick and Cook, 2008). Ca^{2+} signaling is required for every stage of the eukaryotic cell cycle, including activation and expression of transcriptional factors and cyclin-dependent kinases that are necessary for cell-cycle progression (Hogan et al., 2003; Roderick and Cook, 2008), as well as centrosome duplication and separation (Fukasawa, 2007; Matsumoto and Maller, 2002). Crosstalk with other signaling mechanisms, such as the Ras pathway, regulates cell-cycle transition and cell proliferation (Cook and Lockyer, 2006; Cullen and Lockyer, 2002). Dynamic regulation of Ca^{2+} signaling is achieved by cooperation of various cellular components including receptors, channels, transporters, buffering proteins, and downstream effectors (Berridge et al., 2003). Thus, inappropriate activation of Ca^{2+} influx channels or downregulation of Ca^{2+} efflux and sequestration mechanisms could increase basal Ca^{2+} to augment Ca^{2+} signaling and tumor cell proliferation. Alternatively, changes that deplete the endoplasmic reticulum (ER) Ca^{2+} store can confer cellular resistance to apoptosis (Monteith et al., 2007).

In most nonexcitable cells, depletion of ER stores elicits sustained Ca^{2+} influx by store-operated Ca^{2+} (SOC) entry, defining the major Ca^{2+} influx pathway. Upon the stimulation of cell-surface receptors, depletion of ER Ca^{2+} results in release of Ca^{2+} from lumenal EF hand domains of ER-localized STIM proteins, triggering their translocation to ER-plasma membrane junctions where they bind and activate Orai1, the pore subunit of the Ca^{2+} release-activated Ca^{2+} (CRAC) channel, and resulting in refilling of ER stores (Cahalan et al., 2007; Gwack et al., 2007; Lewis, 2007; Vig and Kinet, 2007). Store-operated Ca^{2+} influx is essential for maintaining ER Ca^{2+} content at a precise level and functions in various physiological processes such as gene transcription, cell-cycle progression, and apoptosis (Parekh and Putney, 2005). Dysfunction of store-operated Ca^{2+} signaling mediated by STIM and Orai1 leads to inhibition of physiological and pathophysiological activities including breast tumor cell migration and tumor metastasis (Yang et al., 2009), vascular smooth muscle cell proliferation and migration (Potier et al., 2009), and T cell activation and tolerance (Oh-Hora et al., 2008).

The Secretory Pathway Ca^{2+}-ATPases (SPCA) are ATP-powered pumps that deliver Ca^{2+} and Mn^{2+} ions into the Golgi lumen for protein sorting, processing, and glycosylation (Durr et al., 1998). In higher vertebrates, including human, this essential function is carried out by the ubiquitously expressed SPCA1 isoform, with orthologs in lower eukaryotes including yeast, nematode, and fruit fly (Missiaen et al., 2007). A closely related second

isoform, SPCA2, shares similar transport characteristics and appears at first glance to have a redundant role, given its absence in lower eukaryotes (Vanoevelen et al., 2005; Xiang et al., 2005). The limited tissue distribution of SPCA2 includes mammary epithelium, where it is sharply upregulated during lactation. Whereas SPCA1 showed a modest 2-fold induction upon lactation, SPCA2 increased by 35-fold and was localized to the lumenal secretory cells of the mammary gland (Faddy et al., 2008).

We hypothesized that transformation of mammary epithelial cells to a cancerous phenotype would be accompanied by dysregulation of Ca^{2+} transporters and their downstream signaling pathways, augmenting proliferation and tumor formation. Furthermore, localized, inappropriate secretion of Ca^{2+} in the absence of calcium buffers could result in microcalcifications that appear as radiographic ''signatures'' on mammograms used in diagnosis of breast cancer (Morgan et al., 2005). Although microcalcifications have been extensively used to characterize abnormalities in the breast tissue, a mechanistic understanding of the source of calcium and the specific pathways that lead to their deposition has remained elusive.

In this study, we show that SPCA2 elicits constitutive Ca^{2+} signaling, mediated by Orai1, which correlates with oncogenic activities of mammary tumor cells. Unexpectedly, SPCA2-induced Ca^{2+} signaling was independent of its Ca^{2+} pump activity, and not regulated by store depletion or STIM proteins. SPCA2 interacted with Orai1 by its N terminus and activated Ca^{2+} influx by the C terminus. These findings reveal a Ca^{2+} signaling mechanism in which Orai1 mediates store-independent Ca^{2+} influx, and dysregulation of SPCA2 constitutively activates this pathway leading to oncogenic activity of tumor cells.

RESULTS

Upregulation of SPCA2 Induces Oncogenic Signaling in Mammary Tumor Cells

We used quantitative RT-PCR to investigate the expression of SPCA isoforms in a range of breast cancer-derived and nonmalignant mammary epithelial cells. In contrast to comparable mRNA levels of SPCA1, SPCA2 was highly upregulated in lumenal-like breast cancer-derived cell lines (Figure 1A). Examination of mRNA levels in breast tissue from a small pool of breast cancer patients confirmed this upregulation (Figure 1B) and prompted us to mine data from microarray profiles of 295 primary human breast tumors: highest levels of SPCA2 were found in $ERBB2^{+}$ tumors, among five transcriptional subtypes (Figure S1 available online). Consistent with mRNA levels, protein expression of SPCA2 was higher in MCF-7 cells, a human breast adenocarcinoma cell line, relative to MCF-10A, a nonmalignant human mammary epithelial cell line; in contrast, there was no increase in SPCA1 expression in MCF-7 (Figure 1C). We used lentiviral delivery of shRNA constructs to knock down expression of endogenous SPCA proteins in MCF-7 cells (Figure 1D). Proliferation was inhibited in $SPCA2^{KD}$ cells, with growth rates slower than mock-transduced cells, and similar to cells growing in low extracellular Ca^{2+} ($\sim$0.1 mM). In contrast, $SPCA1^{KD}$ did not cause this growth phenotype (Figure 1E). The RAS-RAF-MEK-ERK1/2 pathway is known to play an essential role in cell proliferation and survival. Phosphorylation of ERK1/2 drives activation of transcriptional factors and expression of downstream proteins such as cyclin D1, which is essential for completion of the G1/S transition (Coleman et al., 2004; Roderick and Cook, 2008). Levels of phospho-ERK and cyclin D1 reduced dramatically in $SPCA2^{KD}$ cells, as well as in cells incubated in low extracellular Ca^{2+}, relative to control cells (Figure 1F).

We examined the effects of depleting endogenous SPCA2 on the transformed phenotype of MCF-7 cells by monitoring growth of cells in soft agar. Fewer and smaller colonies were observed in soft agar seeded with $SPCA2^{KD}$ cells compared to control cells, and normalized results showed a clear reduction of growth in $SPCA2^{KD}$ cells (Figure 1G). Conversely, overexpression of SPCA2 in nontumorigenic MCF-10A cells conferred the ability to form colonies in soft agar (Figure 1H) and increased proliferation rate (Figure 1I). We also monitored tumor generation in nude mice injected subcutaneously in the flank with control or $SPCA2^{KD}$ MCF-7 cells. We show that $SPCA2^{KD}$ conferred only sporadic and delayed tumor formation relative to control (Figure 1J).

To determine whether oncogenic activity of endogenous SPCA2 was mediated by Ca^{2+} signaling, we measured basal cytoplasmic Ca^{2+} levels in control MCF-7 and $SPCA2^{KD}$ cells. We showed significant reduction of intracellular Ca^{2+} levels in $SPCA2^{KD}$ cells and in cells growing in low extracellular Ca^{2+}, but not in $SPCA1^{KD}$ cells (Figure 1K). On the other hand, overexpression of SPCA2 in MCF-10A cells significantly increased basal Ca^{2+} concentration (Figure 1L). Although basal Ca^{2+} levels varied between cell lines, these levels could be modulated by SPCA2 expression levels. Thus, SPCA2 appears to play a role in regulating basal Ca^{2+}, and upregulation of SPCA2 results in constitutive increase of basal Ca^{2+} and cell proliferation associated with oncogenesis.

SPCA2 Elicits Constitutive Ca^{2+} Signaling Independent of Transport Function

To investigate the molecular basis of SPCA2-induced Ca^{2+} signaling, we began by monitoring Ca^{2+}-dependent localization of the nuclear factor of activated T cells, NFAT (Crabtree and Olson, 2002; Huang et al., 2006), in HEK293 cells where expression of SPCA2 is relatively low (Figure S2A). In resting cells, GFP-tagged NFAT localized exclusively in the cytoplasm. Following treatment with thapsigargin, a blocker of sarco/endoplasmic reticulum Ca^{2+}-ATPases (SERCA), depletion of ER Ca^{2+} resulted in store-operated Ca^{2+} entry, elevation of basal Ca^{2+} level, and nuclear translocation of NFAT-GFP in nearly 100% of cells, as expected (Figures 2A and 2B). Whereas transient expression of SPCA1 in HEK293 cells did not alter cytoplasmic localization of NFAT-GFP under resting conditions, transient expression of SPCA2 elicited nuclear translocation of NFAT-GFP in $\sim$75% of cells. This was inhibited by store-operated Ca^{2+} channel blockers, miconazole (Clementi and Meldolesi, 1996), and 2-APB (Parekh and Putney, 2005) at the reported concentrations, and in low extracellular Ca^{2+}, indicating Ca^{2+} entry through plasma membrane Ca^{2+} channels. Inhibition of the Ca^{2+}-activated Ser/Thr phosphatase calcineurin by FK506 also prevented nuclear relocalization of NFAT-GFP in SPCA2-transfected cells (Figures 2A and 2B). Accordingly, NFAT was predominantly

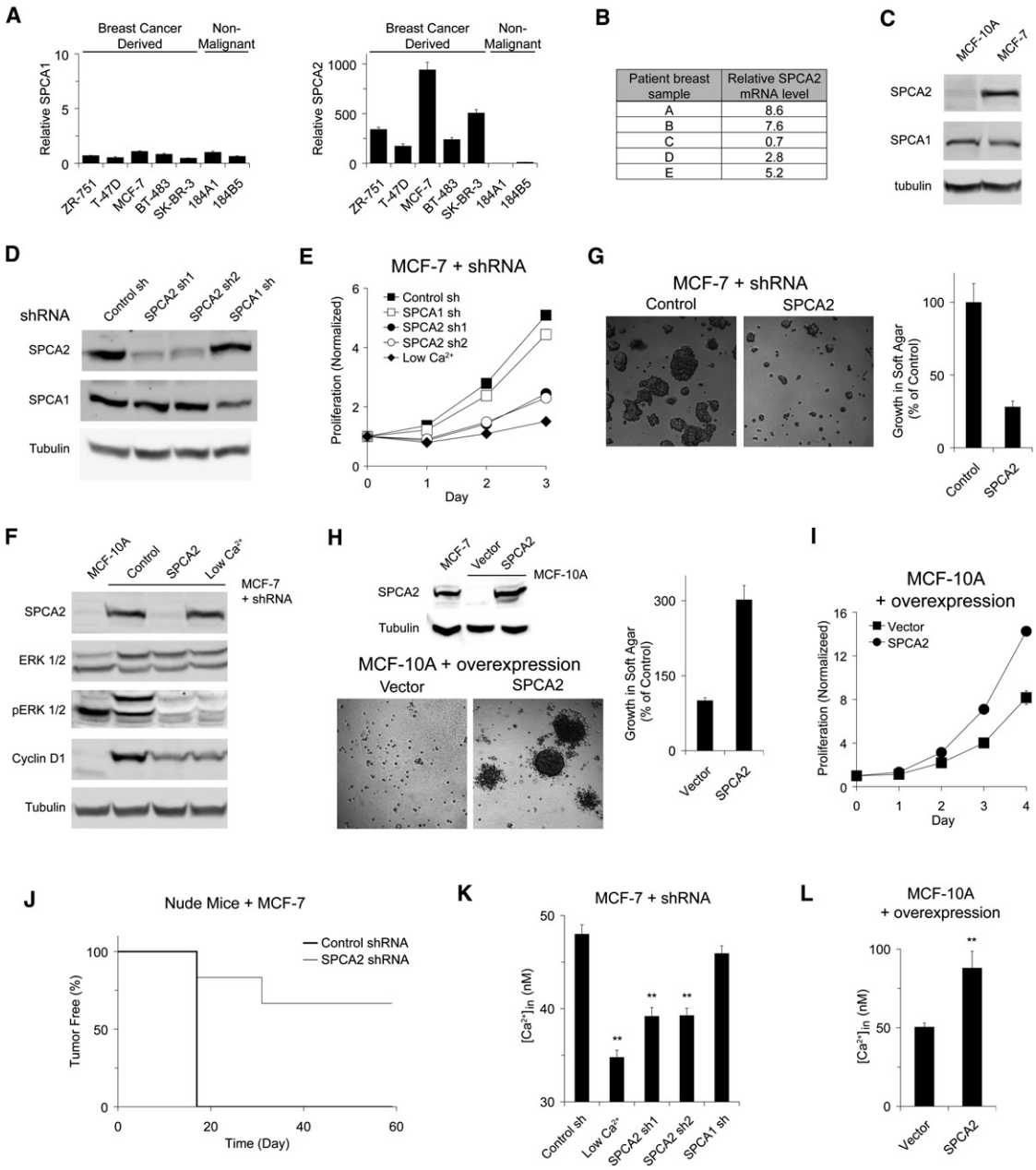

Figure 1. Upregulation of SPCA2 Induces Oncogenic Signaling in Mammary Tumor Cells

mRNA levels were measured by quantitative real-time RT-PCRs and normalized to 18S rRNA in (A) a panel of breast epithelial cell lines relative to 184A1 and (B) in human breast tumor samples compared to matched normal surrounding breast tissue. n = 3 in (A).

(C) Immunoblot of SPCA expression in MCF-10A and MCF-7 cells.

Immunoblot (D) and normalized proliferation (E) of MCF-7 cells lentivirally transduced with shRNA against SPCA isoforms are shown. n = 3 in (E).

(F) Immunoblot of ERK 1/2 phosphorylation and cyclin D1 expression in MCF-7 cells transduced with shSPCA2.

Micrographs and normalized growth of (G) MCF-7 cells with SPCA2 knockdown or (H) MCF-10A cells with SPCA2 overexpression in soft agar are shown; n = 3. Immunoblot showing relative SPCA2 expression levels is shown in (H).

(I) Normalized proliferation of MCF-10 cells with SPCA2 overexpression; n = 3.

(J) Tumor incidence in nude mice injected with MCF-7 cells; n = 6, p = 0.005 (log-rank test).

(K) Basal Ca^{2+} levels in MCF-7 cells with SPCA2 knockdown. From left to right: n = 80, 80, 77, 81, 69. **p < 0.01 (Student's t test).

(L) Basal Ca^{2+} levels in MCF-10A cells with SPCA2 overexpression. Vector, n = 23; SPCA2, n = 23. **p < 0.01 (Student's t test).

Error bars represent standard error (K and L) or standard deviation (A, E, G, H, and I).

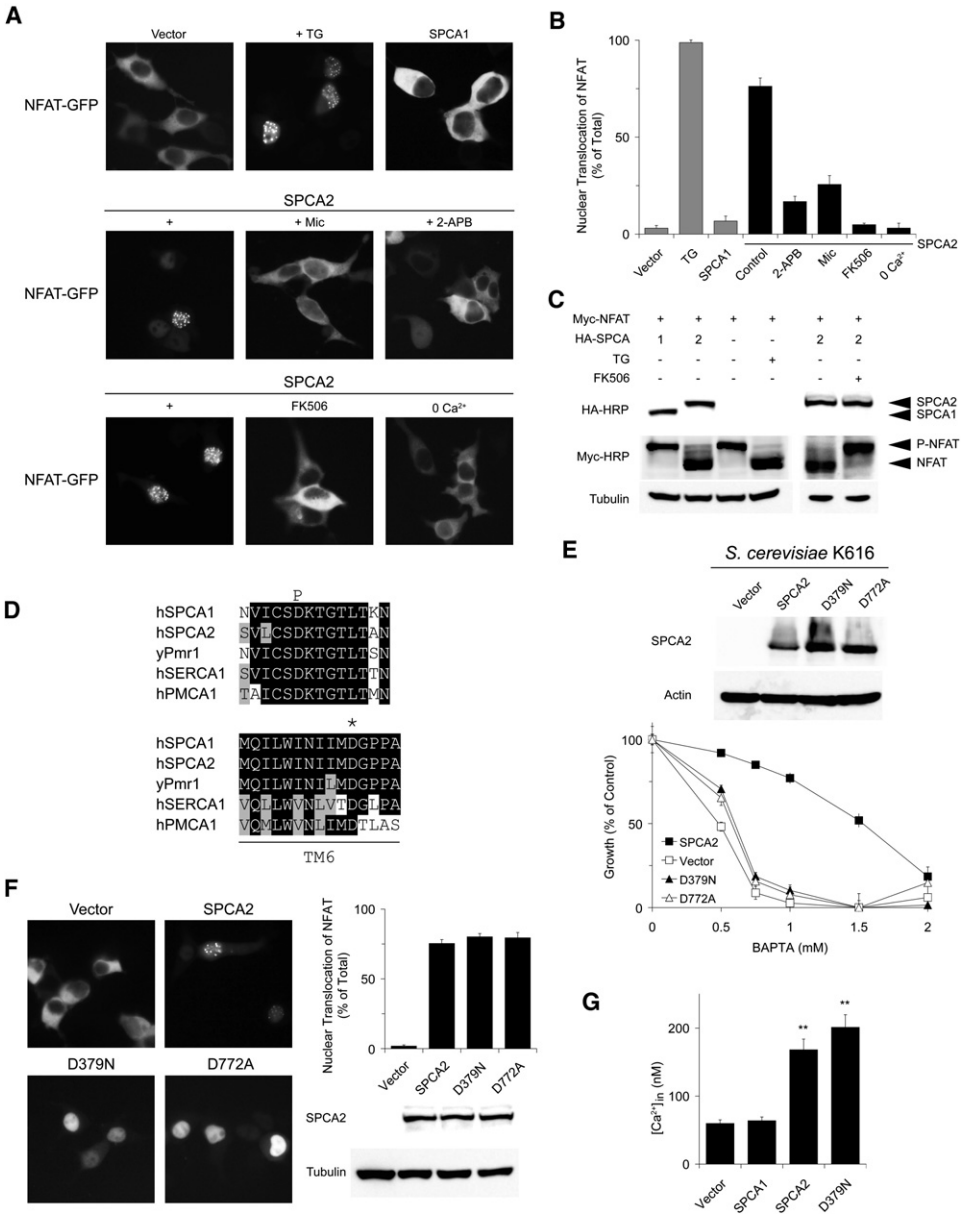

Figure 2. SPCA2 Elicits Constitutive Ca^{2+} Signaling Independent of Transport Function

Representative live images (A) and quantification of nuclear localization (B) of NFAT-GFP in HEK293 cells transfected with SPCA1 or SPCA2, or treated with drugs. n = 3 in (B).

(C) Immunoblot showing phosphorylation status of NFAT following expression of SPCA1or SPCA2 or treatment with thapsigargin (TG) or FK506.

(D) Alignments showing conserved aspartates in phosphorylation (*P*) domain (D379 in SPCA2) or transmembrane helix 6 (D772 in SPCA2) of P-type Ca^{2+}-ATPases.

(E) Immunoblot and normalized growth of yeast K616 expressing SPCA2 or mutants D379N and D772A in BAPTA medium; n = 4.

(F) Representative live images, quantification of NFAT translocation in HEK293 cells, and immunoblot showing expression of SPCA2 WT or mutants; n = 3.

(G) Basal Ca^{2+} levels in HEK293 cells expressing SPCA1, SPCA2, or D379A mutant. From left to right, n = 57, 47, 46, 44. **p < 0.01 (Student's t test).

Error bars represent standard error (G) or standard deviation (B, E, and F).

dephosphorylated in TG-treated- or SPCA2-expressing cells but remained phosphorylated in cells transfected with SPCA1 or empty vector and in FK506-treated cells (Figure 2C).

These findings were unexpected, given the known function of SPCA2 in pumping Ca^{2+} away from the cytoplasm into Golgi/vesicular stores. To determine whether constitutive Ca^{2+} signaling elicited by SPCA2 was dependent on its Ca^{2+} pumping ability, we generated two variants: mutant D379N lacks the conserved and essential aspartate that is transiently phosphorylated by ATP in the catalytic cycle, and mutant D772A disrupts

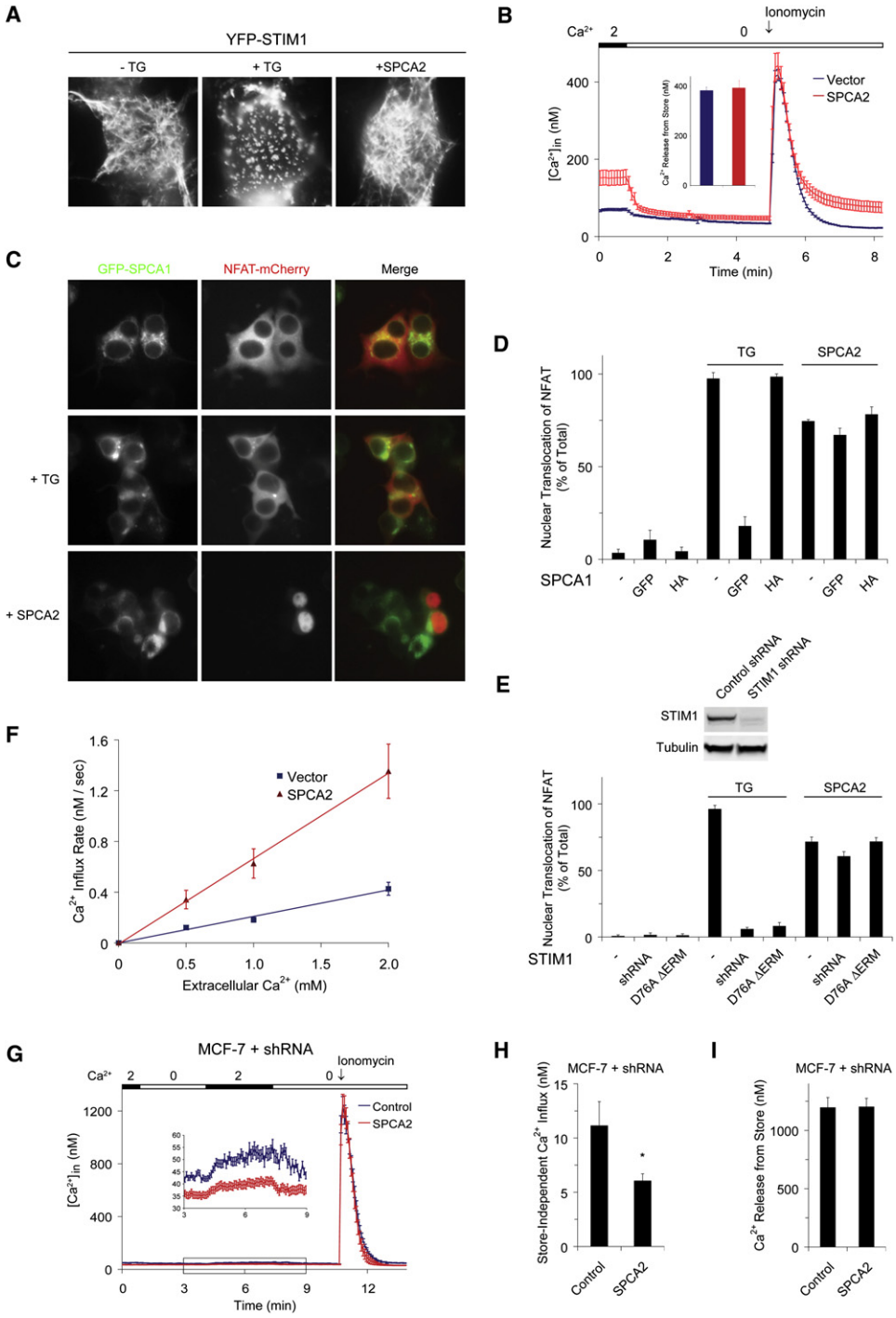

Figure 3. SPCA2-Mediated Ca^{2+} Signaling Is Store Independent

(A) Localization of YFP-STIM1 in HEK293 cells following TG treatment or SPCA2 expression.

(B) Representative Ca^{2+} traces following emptying of stores with 2 μM Ionomycin in HEK293 cells with or without SPCA2 expression. Vector, n = 40; SPCA2, n = 25. Cells were cultured in low Ca^{2+} medium (~0.1 mM) after transfection, followed by a 30 min incubation in normal Ca^{2+} (2 mM) immediately before calcium imaging experiments to allow restoration of stores (as described in Extended Experimental Procedures—Calcium imaging).

(C) Representative images of GFP-SPCA1 and NFAT-mCherry following TG treatment or SPCA2 expression in HEK293 cells and (D) quantification of nuclear NFAT-mCherry translocation. n = 3 in (D).

(E) Quantification of NFAT nuclear translocation following STIM1 knockdown or expression of dominant-negative STIM1 mutant in cells treated with TG or expressing SPCA2; n = 3.

a conserved and essential Ca^{2+}-binding site (Figure 2D) (Wei et al., 2000). Both mutants failed to rescue growth of a yeast strain lacking endogenous Ca^{2+} pumps in BAPTA-supplemented medium, consistent with loss of Ca^{2+}-ATPase activity (Figure 2E), but retained ability to elicit constitutive NFAT translocation in HEK293 cells (Figure 2F). Also, mutant D379N induced growth of MCF-10A in soft agar similar to wild-type (WT) SPCA2 (Figure S2B). Furthermore, introduction of SPCA2, either WT or D379N mutant, resulted in elevated basal cytoplasmic Ca^{2+} levels in HEK293 cells, relative to cells transfected with empty vector or SPCA1 (Figure 2G). This was reminiscent of the effect of upregulation of endogenous SPCA2 on basal Ca^{2+} levels in MCF-7 cells (Figure 1K). We conclude that SPCA2, but not SPCA1, induces constitutive Ca^{2+} influx and signaling by a mechanism that is independent of its known function as a Ca^{2+}-ATPase.

SPCA2-Mediated Ca^{2+} Signaling Is Store Independent

To investigate the possibility that SPCA2 could elicit ER Ca^{2+} store depletion leading to constitutive store-operated Ca^{2+} entry (SOCE), we examined the status of the ER Ca^{2+} store. YFP-STIM1, the ER-localized Ca^{2+} sensor protein, was present in a reticular, ER-like pattern in resting cells and redistributed to punctae after store depletion with thapsigargin (Liou et al., 2005), as expected (Figure 3A). Transient transfection with SPCA2 did not elicit puncta formation of YFP-STIM1, suggesting that the ER store was not Ca^{2+} depleted (Figure 3A). Next, we directly measured the ER Ca^{2+} content by ionomycin treatment to completely release Ca^{2+} from intracellular stores. In Ca^{2+}-free medium, peak levels of Ca^{2+} released by ionomycin were identical in cells transfected with SPCA2 or empty vector (Figure 3B and Figures S3A and S3B). In a different, independent approach, we used a thapsigargin-insensitive, ER-localized Ca^{2+}-ATPase to ensure that intracellular ER stores were replete with Ca^{2+}. N-terminal GFP-tagged SPCA1 partially mislocalized to the ER (Figure S3C) where it is functional in filling the stores and preventing nuclear translocation of NFAT-mCherry after thapsigargin treatment (Figure S3D and Figures 3C and 3D). Despite coexpression with ER-localized GFP-SPCA1, SPCA2 was capable of eliciting nuclear translocation of NFAT-mCherry (Figures 3C and 3D). HA-tagged SPCA1 localizes to the Golgi (Figure S3C) and does not interfere with thapsigargin-induced SOCE, nor with SPCA2-induced nuclear translocation of NFAT-mCherry (Figure 3D), indicating that Ca^{2+} signaling by SPCA2 is also independent of Golgi stores. It was previously reported that knockdown of STIM1 or expression of the dominant-negative mutant D76A ΔERM blocked SOC signaling (Huang et al., 2006; Roos et al., 2005), as seen by the failure of TG to elicit nuclear translocation of NFAT (Figure 3E and Figures S3E and S3F). Also, knockdown of STIM2, the feedback regulator of cytosolic and ER Ca^{2+} levels, was shown to lower basal Ca^{2+} concentration (Brandman et al., 2007) (Figures S3E and S3G). However, despite expression of dominant-negative D76A ΔERM or knockdown of STIM1 and STIM2 expression, either singly or in combination, SPCA2 retained the ability to increase basal Ca^{2+} concentration and cause NFAT-GFP translocation to the nucleus, evidently by a STIM-independent Ca^{2+} signaling mechanism (Figure 3E and Figures S3F and S3G). We showed that SPCA2 expression in HEK293 cells resulted in Ca^{2+} influx from the extracellular medium, as shown by Mn^{2+} quench of intracellular preloaded Fura-2 as well as $^{45}Ca^{2+}$ uptake (Figures S4A and S4B). Initial rates of uptake, monitored within the first 60 s, were significantly increased by expression of SPCA2 (Figure 3F and Figures S4D–S4I). Additionally, measurement of $^{45}Ca^{2+}$ efflux and Fura2 fluorescence confirmed that SPCA2-induced elevation of intracellular Ca^{2+} did not result from decreased rates of Ca^{2+} efflux (Figures S4C–S4F). Consistent with these findings, knockdown of endogenous SPCA2 in MCF-7 cells also diminished store-independent Ca^{2+} entry without changing internal Ca^{2+} stores (Figures 3G–3I). Taken together, our results reveal a mechanism for SPCA2-mediated Ca^{2+} signaling that is independent of both ER and Golgi Ca^{2+} stores.

SPCA2 Interacts with Orai1 to Mediate Ca^{2+} Entry

Our results suggested that SPCA2 elicited Ca^{2+} influx through plasma membrane Ca^{2+} channels. Immunofluorescence and cell-surface biotinylation showed partial localization of endogenous SPCA2 to the plasma membrane in MCF-7 cells, where it has the potential to elicit Ca^{2+} influx (Figures 4A and 4B). Next, we sought evidence for physical interaction between SPCA2 and candidate Ca^{2+} channels. Although SPCA2-mediated Ca^{2+} influx was independent of ER stores, we observed coimmunoprecipitation of the endogenous store-operated channel Orai1 and native SPCA2 in MCF-7 cells (Figure 4C). We verified and extended these findings using epitope-tagged proteins expressed in HEK293 cells: we could document robust coimmunoprecipitation of Orai1-Myc and HA-SPCA2 (Figure 4D). Consistent with the specificity of the Orai1-SPCA2 interaction, HA-SPCA1 did not coimmunoprecipitate with Orai1 (Figure 4D). Similar to endogenous protein, up to 10% of HA-SPCA2 could be labeled by cell-surface biotinylation, including both WT and the pump-inactive D379N mutant; in contrast, SPCA1 was barely detectable (Figure 4E). Surface residence of SPCA2 correlated with total expression levels, and with elevation of basal Ca^{2+} (Figure S5A). We also used cell-surface biotinylation to confirm that a portion of SPCA2-complexed Orai1 was found at the plasma membrane (Figures S5B and S5C). Although SPCA2 preferentially interacted with lower molecular weight bands of posttranslationally modified Orai1 as has been reported for STIM1 (Park et al., 2009; Vig et al., 2006), we confirmed that all forms of Orai1 reached the plasma membrane where they could be biotinylated (Figure 4B). Epitope-tagged SPCA2 and Orai1 also partially colocalized by confocal immunofluorescence

(F) Initial rates of Ca^{2+} influx in HEK293 cells with or without SPCA2 expression, calculated from the experiments shown in Figure S4, with 0.5 mM, 1.0 mM, or 2.0 mM extracellular Ca^{2+}. Vector: n = 30 (0.5 mM), 25 (1.0 mM), 28 (2.0 mM); SPCA2: n = 28 (0.5 mM), 23 (1.0 mM), 25 (2.0 mM).

Representative Ca^{2+} traces (G) and average intracellular Ca^{2+} concentration representing store-independent Ca^{2+} influx (H) and internal Ca^{2+} store content (I) in $Control^{KD}$ and $SPCA2^{KD}$ MCF-7 cells. $Control^{KD}$, n = 36; $SPCA2^{KD}$, n = 30. *$p < 0.05$ (Student's t test).

Error bars represent standard error (B, F, G, H, and I) or standard deviation (D and E).

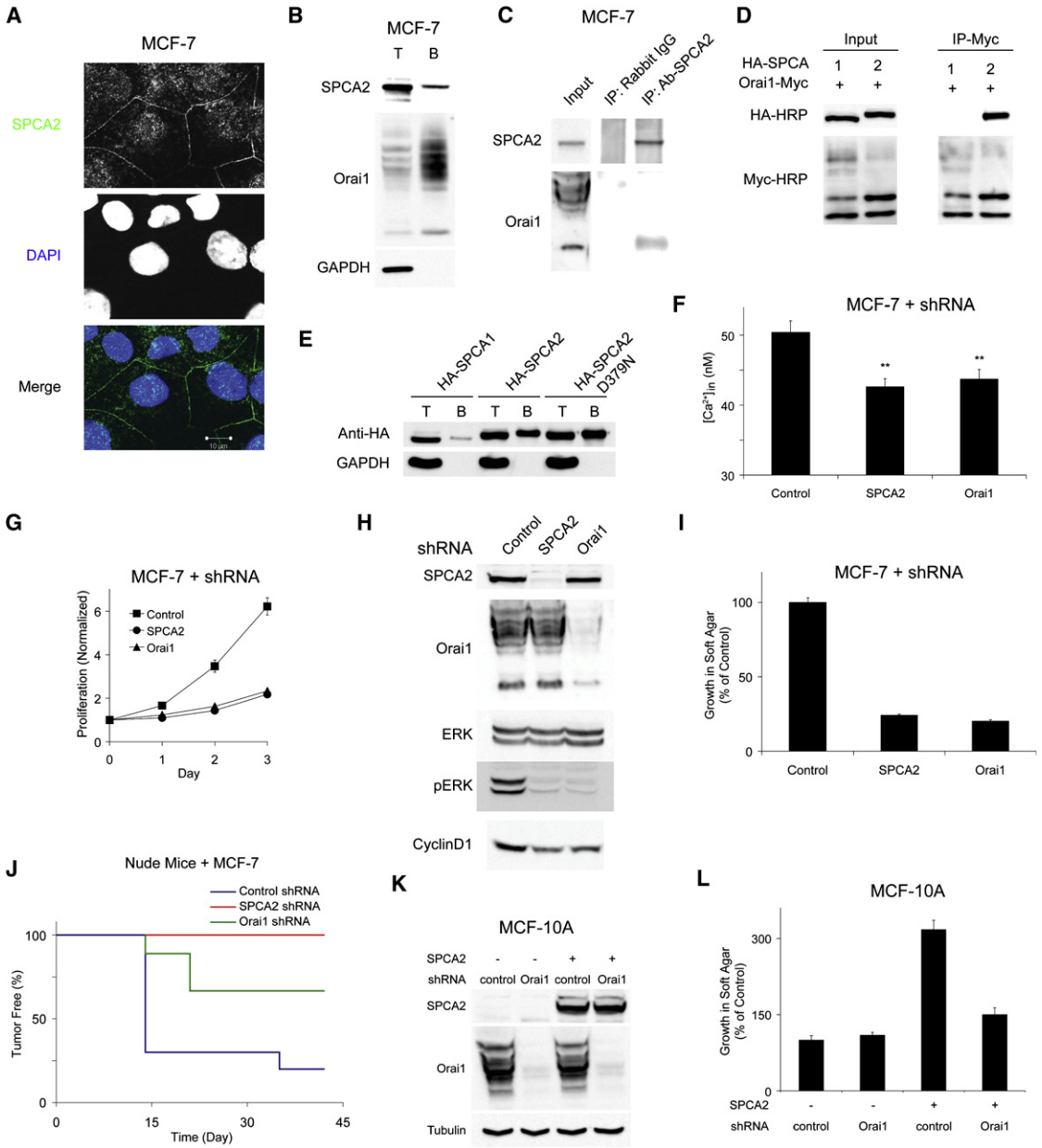

Figure 4. SPCA2 Interacts with Orai1 to Mediate Ca^{2+} Entry

(A) Confocal micrographs of immunofluorescence staining of endogenous SPCA2 in MCF-7 cells showing partial plasma membrane localization.
(B) Cell-surface biotinylation of endogenous SPCA2 and Orai1 in MCF-7 cells. T and B represent total lysate and biotinylated fraction, respectively.
(C) Coimmunoprecipitation of endogenous SPCA2 and Orai1 in MCF-7 cells.
(D) Coimmunoprecipitation of HA-SPCA with Orai1-Myc following expression in HEK293.
(E) Cell-surface biotinylation of HA-tagged SPCA1, SPCA2, or D379N SPCA2 expressed in HEK293.
(F) Basal Ca^{2+} in MCF-7 cells after knockdown of endogenous SPCA2 or Orai1. $Control^{KD}$, n = 47; $SPCA2^{KD}$, n = 54; $Orai1^{KD}$, n = 52. **$p < 0.01$ (Student's t test).
(G) Normalized proliferation of MCF-7 cells with SPCA2 or Orai1 knockdown; n = 3.
(H) Immunoblot of ERK 1/2 phosphorylation and cyclin D1 expression in MCF-7 cells with SPCA2 or Orai1 knockdown.
(I) Normalized growth of MCF-7 cells with SPCA2 or Orai1 knockdown in soft agar; n = 3.
(J) Tumor incidence in nude mice injected with MCF-7 cells; $control^{KD}$, n = 10; $SPCA2^{KD}$, n = 8, p = 0.007 (log-rank test); $Orai1^{KD}$, n = 9, p = 0.045 (log-rank test).
Immunoblot (K) and normalized growth in soft agar (L) of MCF-10A cells with knockdown of Orai1 in control and cells overexpressing SPCA2. n = 3 in (L).
Error bars represent standard error (F) or standard deviation (G, I, and L).

microscopy (Figure S5D). Unlike STIM (Yeromin et al., 2006), interaction between SPCA2 and Orai1 was not affected by store depletion with thapsigargin, consistent with a store-independent regulation of Orai1 function (Figure S5E). Supporting this possibility, neither WT STIM1 nor the constitutively active STIM1 mutant (D76A) (Huang et al., 2006; Liou et al., 2005) was in the same protein complex as SPCA2 (Figure S5F). These findings point to Orai1 as a likely candidate for mediating SPCA2-regulated, store-independent Ca^{2+} influx in breast cancer cells.

To evaluate this possibility, we suppressed the expression of endogenous Orai1 in MCF-7 cells: $Orai1^{KD}$ lowered basal Ca^{2+} to levels comparable to those seen upon depleting endogenous SPCA2 (Figure 4F). In addition, $Orai1^{KD}$ in MCF-7 cells suppressed cell proliferation (Figure 4G) and inhibited the RAS pathway, as did $SPCA2^{KD}$ (Figure 4H and Figure S5G). Furthermore, $Orai1^{KD}$ suppressed colony formation in soft agar, to a similar extent as $SPCA2^{KD}$ (Figure 4I), and tumor generation in nude mice (Figure 4J). Simultaneous knockdown of both Orai1 and SPCA2 did not confer additive phenotypes (Figures S5H, S5J, and S5K). In MCF-10A cells overexpressing SPCA2, cell transformation and elevation of basal Ca^{2+} level were reversed by knockdown of Orai1, consistent with a role for Orai1 downstream of SPCA2 (Figures 4K–4L and Figure S5L). As expected for a store-independent mechanism of Orai1 activation, depletion of STIM1 (Figures S5M–S5O) or STIM2 (Figures S5I–S5K), the upstream activators of Orai1 in SOCE signaling, did not confer comparable phenotypes in MCF-7 cells. Taken together, our data point to promotion of tumorigenic pathways by SPCA2 in breast cancer cells, mediated by interaction with Orai1.

Amino Terminus of SPCA2 Interacts with Orai1

To dissect the molecular determinants of the SPCA2-Orai1 interaction, we evaluated the efficiency of coimmunoprecipitation between a series of SPCA chimeric proteins and Orai1. In each case, the ability of a chimeric protein to coimmunoprecipitate with Orai1 correlated with ability to elicit NFAT translocation, suggesting that physical interaction between the two proteins was required for Ca^{2+} signaling. Chimeras containing the SPCA2 N terminus showed stronger binding with Orai1 and more effective NFAT translocation (Figures 5A–5C).

Next, we examined physical interaction between Orai1 and major intracellular soluble domains of SPCA2, including N and C termini and the large intracellular loop, which contains the iconic aspartate of P-type ATPases (D379). Of these, only the N terminus was able to pull down Orai1 (Figure 5D). To further map regions within the SPCA2 N terminus responsible for binding to Orai1, we performed GST pull downs between Orai1 and a series of SPCA1 and SPCA2 fragments. The SPCA1 N terminus did not bind to Orai1, consistent with an absence of functional interaction between SPCA1 and Orai1 (Figure 5E). A region of 40 amino acids within the N terminus of SPCA2 was able to effectively interact with Orai1 (Figure 5E; construct SPCA2N-8, aa 67–106). Surprisingly, this region was highly conserved between the two isoforms, with ~50% amino acid identity (Figure S6A). We therefore conducted mutational replacement of amino acids in the SPCA2 N terminus with the equivalent residues in SPCA1 and identified four amino acids that together were critical for interaction between the SPCA2 N terminus and Orai1 (Figure 5F). Three-dimensional structure of the SPCA2 N terminus, predicted by I-TASSER server (Wu et al., 2007), suggested that Val71, Thr75, and Ser78 were spatially clustered, whereas Val95 was on the remote side (Figure 5G, Figures S6B and S6C, and Table S1).

Finally, we evaluated the effect of Orai1 expression on the intracellular localization of N-terminal fragments of SPCA1 and SPCA2 in HEK293 cells. When expressed alone, both fragments were localized intracellularly, with the SPCA1 N-terminal fragment diffusely distributed in the cytosol, and the SPCA2 N terminus concentrated in the perinuclear region. Although the coexpression of Orai1 did not change localization of the SPCA1 N terminus, there was a redistribution of the SPCA2 N terminus to the cell surface, providing additional evidence that the N-terminal domain of SPCA2, but not SPCA1, interacts physically with Orai1 (Figure 5H).

Cooperation of SPCA2 N and C Termini in Ca^{2+} Signaling

We further investigated the molecular mechanism of SPCA2-activated Ca^{2+} signaling. We noticed that the isolated N terminus of SPCA2 did not elicit NFAT translocation despite being able to interact directly with Orai1, while the C terminus was sufficient to induce NFAT translocation when it was linked to two or more transmembrane domains and targeted to the membrane (Figure 6A and Figures S7A and S7B). Surprisingly, a similar membrane-anchored construct containing the SPCA1 C terminus was also able to activate constitutive Ca^{2+} signaling even though full-length SPCA1 could not (Figure 6A). In addition, both SPCA1 and SPCA2 membrane-anchored C-terminal domains physically interacted with Orai1 (Figure S7C). We hypothesized that access of the SPCA C terminus to Orai1 was blocked in the full-length proteins, and binding of the SPCA2 N terminus to Orai1 led to exposure of the C terminus and activation of downstream Ca^{2+} signaling. Analysis of deletion and point mutants of the SPCA2 C terminus identified essential functional residues including several positive charges (lysines and arginines) and a putative PDZ binding domain (Figure 6A and Figure S7D), conserved between human, rat, and mouse SPCA proteins (Figure S7E). We then measured intracellular Ca^{2+} concentrations upon expression of SPCA2 C-terminal constructs in HEK293 cells. Basal Ca^{2+} level was elevated dramatically by expression of the SPCA2 C terminus but remained the same as GST control when lysines (arginines) were mutated or the putative PDZ domain was deleted (Figure 6B). The N-terminal domain of SPCA2, but not SPCA1, had a dominant-negative effect, dramatically inhibiting NFAT translocation induced by full-length SPCA2 or the C terminus (Figure 6C), whereas SOCE was not blocked by the SPCA2 N terminus or full-length with the C terminus deleted (SPCA2 Δ924–946) (Figure S7F). Importantly, expression of the membrane-anchored SPCA2 C terminus in MCF-10A cells was able to induce cell transformation, consistent with the fact that it was identified to be the functional domain of SPCA2 and elicited constitutive Ca^{2+} signaling (Figure 6D). STIM1 CRAC activation domain (Park et al., 2009) showed a similar effect, supporting the role of Ca^{2+} signaling in cell transformation (Figures S7G and S7H).

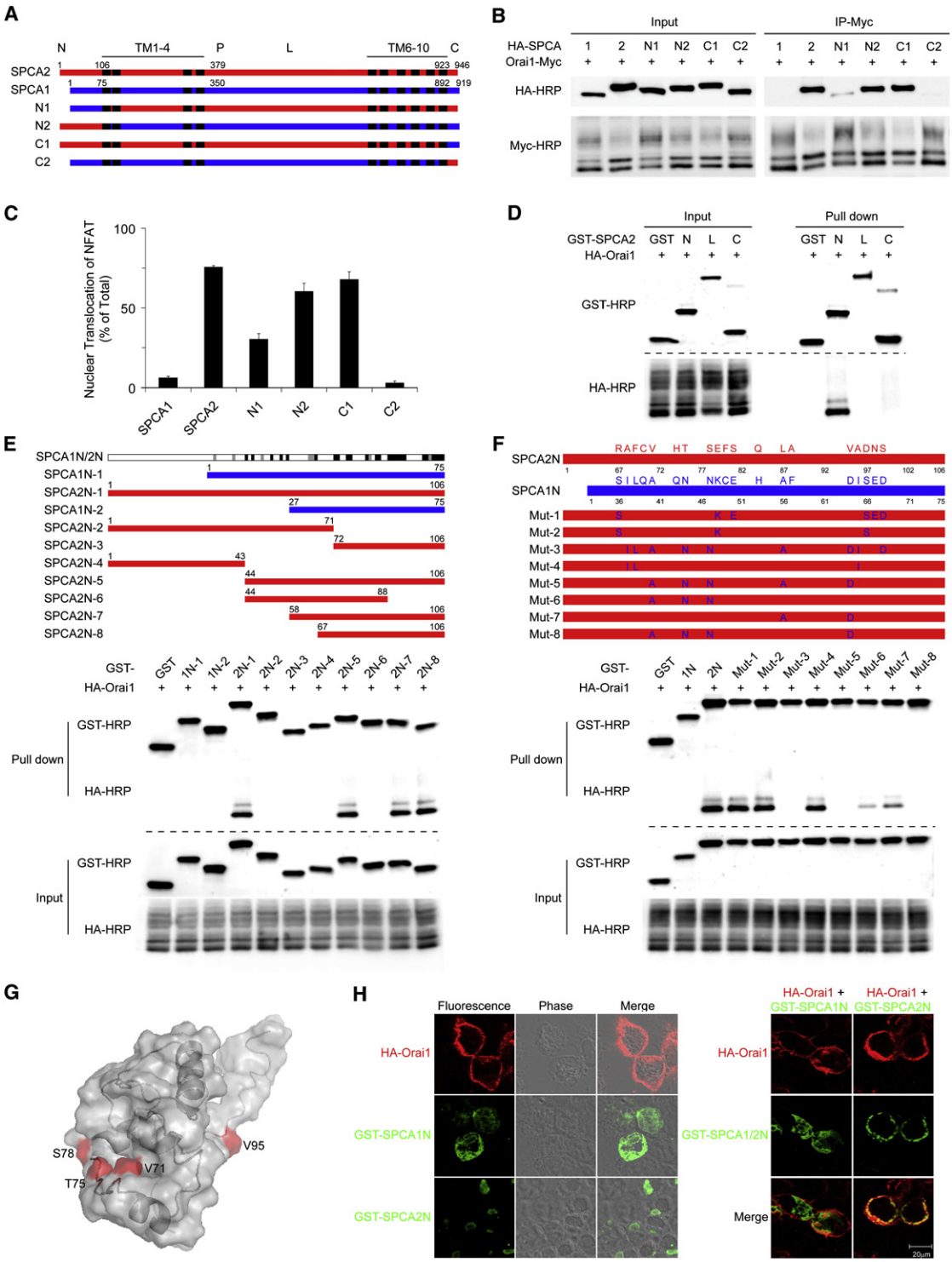

Figure 5. N-Terminal Domain of SPCA2 Interacts with Orai1

(A) Schematic of SPCA chimeras. N1 and C1 have the N and C termini of SPCA2 replaced by corresponding regions of SPCA1. N2 and C2 have N and C termini of SPCA1 replaced by corresponding regions of SPCA2. "P" indicates the conserved aspartate that is transiently phosphorylated by ATP in the catalytic cycle. "L" represents intracellular loop.

(B) Interaction between Orai1 and SPCA chimeras was examined by coimmunoprecipitation in HEK293 cells.

(C) Quantification of NFAT nuclear translocation in HEK293 cells expressing SPCA chimeras described in (B). n = 3; error bars represent standard deviation.

We next expressed GST fusions of various Orai1 domains including N and C termini, extra- and intracellular loops together with full-length SPCA2 or the N-terminal fragment of SPCA2. Both N and C termini, but not the loops of Orai1, were able to pull down both full-length and N terminus of SPCA2, revealing that SPCA2 and Orai1 interacted within the cytoplasm (Figures 6E and 6F). We then mapped subregions of Orai1 N and C termini to further explore SPCA2 interaction domains (Figure 6G). GST pull-down experiments identified a fragment (aa 48–91) of the Orai1 N terminus that bound SPCA2 with a higher affinity than the full-length N terminus. Mutation L273S, previously shown to disrupt the coiled-coil domain of the C terminus of Orai1 (Muik et al., 2008), severely reduced the interaction with SPCA2 (Figure 6G). Taken together, we propose a model for SPCA2 interaction with Orai1 and activation of Ca^{2+} signaling. We suggest that the N terminus of SPCA2 binds Orai1, resulting in a conformational change and exposure of the C terminus, which can interact with Orai1 either directly or together with other proteins to activate Ca^{2+} influx (Figure S7I).

DISCUSSION

Role of SPCA2 and Orai1 in Breast Tumorigenicity

Our findings reveal a mechanism for activation of the so-called SOCE channel Orai1 that is independent of ER and Golgi Ca^{2+} stores and sensors. This store-independent mode of endogenous Orai1 activation in breast cancer-derived MCF-7 cells underlies constitutive Ca^{2+} signaling, proliferation, and anchorage-independent growth and implicates a hitherto unrecognized role for Orai1 in breast tumorigenicity. We also identified a role for SPCA2 in tumorigenicity and revealed a functional link to RAS signaling. The RAS-ERK pathway regulates cell-cycle progression and cell proliferation, and it is well known that hyperactivation of the *RAS* gene family correlates with various human cancers (Bos, 1989). GTP-exchange factors (GEFs) and GTPase-activating proteins (GAPs) control activity of RAS by regulating the balance of GTP binding and hydrolysis (Donovan et al., 2002; Downward, 1996). Recent studies have suggested that GEFs and GAPs can be regulated by different Ca^{2+} signals, such as amplitude of the Ca^{2+} signals and frequency of Ca^{2+} oscillation (Cook and Lockyer, 2006). By monitoring activation of ERK and expression of the downstream protein cyclin D1, we revealed a correlation between SPCA2 and Orai1-mediated increase of basal Ca^{2+} levels and constitutive activation of RAS signaling in MCF-7 cells, placing the SPCA2-Orai1 pathway in the RAS signaling network.

Mechanism of Orai1-Mediated Ca^{2+} Signaling Induced by SPCA2

It has been reported that STIM1 and Orai1 mediate CRAC currents in endothelial cells, and knockdown of either elicits cell-cycle arrest (Abdullaev et al., 2008). Another recent study implicated a store-dependent role for Orai1 in cell migration of the metastatic breast cancer line MDA-MB-231, based on a requirement for STIM1 (Yang et al., 2009). We note that SPCA2 expression is very low in MDA-MB-231 (data not shown), consistent with a Ca^{2+} signaling mechanism distinct from the store-independent pathway reported here. Although the importance of SOC signaling is well established, the store independent Ca^{2+} signaling described in our study suggests that multiple mechanisms may invoke Orai1 activation. Interaction between SPCA2 and Orai1 was not affected by ER store depletion and activation of SOC signaling, and SOCE was not inhibited by expression of SPCA2, supporting that SPCA-induced signaling may function independently of the SOC pathway and different pools or fine subdomains of Orai1 are involved in the two pathways.

ER-localized Ca^{2+} sensor STIM proteins, which regulate SOCE, did not physically interact with SPCA2 or participate in regulation of the SPCA2-Orai1 signaling pathway. In addition, internal Ca^{2+} store content was not depleted by suppression or overexpression of SPCA2. Thus, it remains to be determined how the store-independent, Orai1-mediated mechanism of Ca^{2+} influx is regulated. One possibility is that signaling activity of SPCA2 is regulated by its trafficking between Golgi and plasma membrane. Interaction with Orai1 at the cell surface may be dependent on a specific conformation of SPCA2, which could be regulated by kinase-mediated phosphorylation, Ca^{2+} binding, or changes in pH between extracellular and Golgi lumen. Removal of a potential PDZ-binding motif in the last four residues of the C-terminal tail of SPCA2 abolished Ca^{2+} signaling, suggesting that interaction with scaffold proteins may be important for activation of this signaling pathway.

Based on the function of a series of chimeras and mutant proteins, we propose a model in which cooperation of N and C termini of SPCA2 is required for Orai1-mediated Ca^{2+} signaling. Whereas the N terminus of SPCA2 binds strongly to Orai1, the C terminus elicits activation of Ca^{2+} influx. Although the Orai1-binding domain within the SPCA2 N terminus is highly conserved with the corresponding region of SPCA1, no interaction was detected between the SPCA1 N terminus and Orai1. Replacement of four residues within the minimal Orai1-binding domain of the SPCA2 N terminus (Val71, Thr75, Ser78, and Val95) to the corresponding less hydrophobic or charged residues in SPCA1 abolished the interaction with Orai1.

(D) Interaction between the SPCA2 N terminus (N: aa 1–106), intracellular loop (L: aa 353–733), C terminus (C: aa 923–946), and Orai1 was examined by GST pull-down in HEK293 cells.

(E) Mapping of regions in SPCA1/2 that interact with Orai1. GST-SPCA1/2 N-terminal fragments were coexpressed with HA-Orai1 in HEK293 cells, and interaction with Orai1 was examined by GST pull-down. Sequence conservation between SPCA1 and SPCA2 is shown on top, with black, gray, and white bars representing identical, similar, and different amino acids, respectively, as defined by ClustalW.

(F) Screening of SPCA2 N terminus for amino acids critical for the interaction with Orai1 in HEK293 cells. Point mutations in SPCA2 N terminus convert amino acids to the equivalent residues in SPCA1 N terminus.

(G) Predicted 3D structure of the SPCA2 N terminus with residues essential for interaction with Orai1 shown in red.

(H) Localization of SPCA1/2 N termini, with or without coexpression of Orai1.

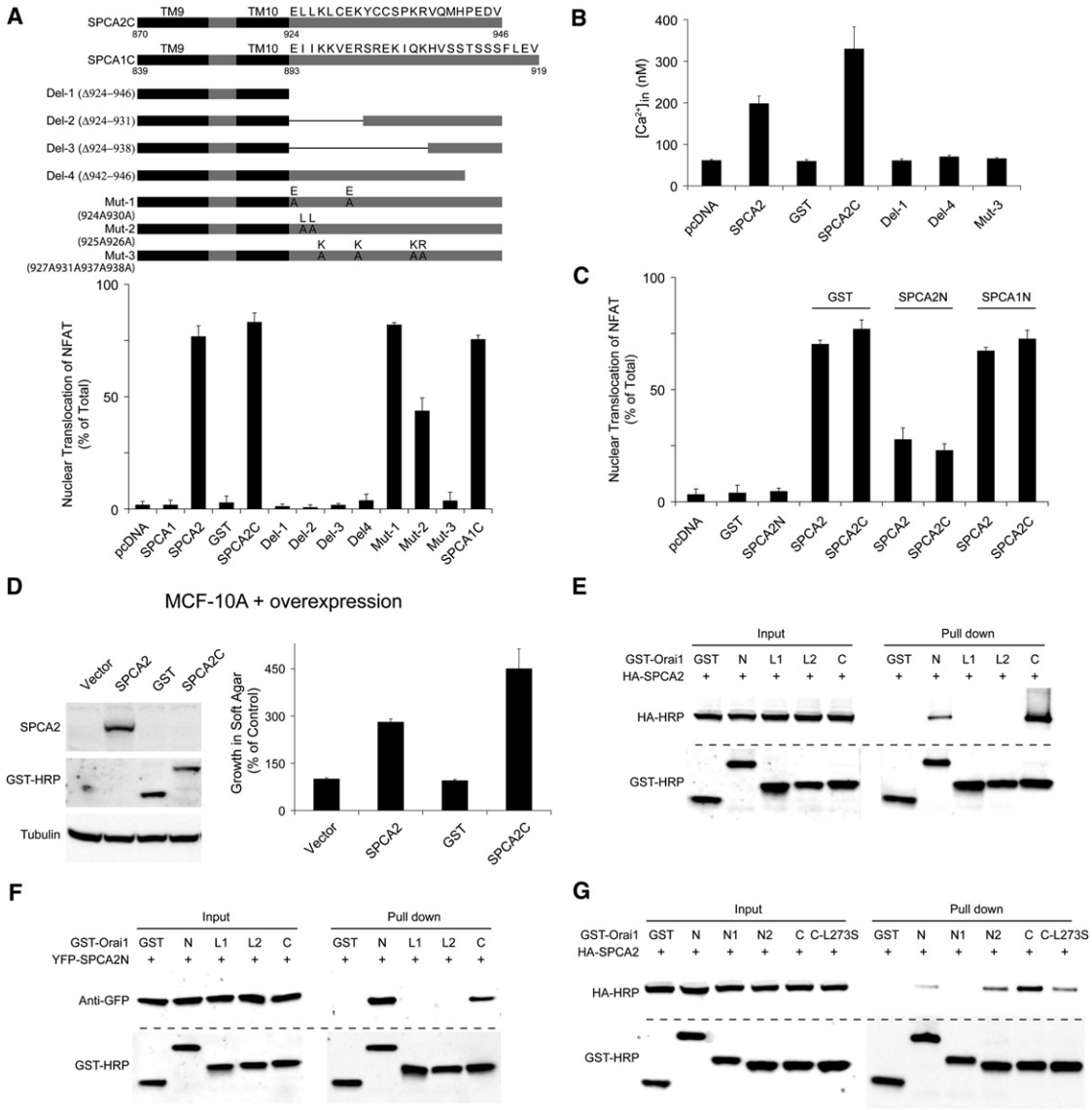

Figure 6. Cooperation of SPCA2 N- and C-Terminal Domains in Ca^{2+} Signaling

(A) SPCA2 C terminus was sufficient to activate Ca^{2+} signaling. Functions of deletion and point mutants of SPCA2 C-terminal domain were examined by NFAT translocation assay in HEK293 cells. Full-length SPCA proteins were HA-tagged, and all C terminus fragments shown were GST-tagged; n = 3.

(B) Basal intracellular Ca^{2+} concentrations in HEK293 cells, with the expression of GST-tagged deletion and point mutants of the SPCA2 C-terminal domain described in (A). From left to right, n = 49, 45, 46, 48, 40, 54, 59.

(C) Effects of N-terminal fragments of SPCA proteins on NFAT translocation induced by SPCA2 full-length or C-terminal fragment shown in (A). n = 3.

(D) Immunoblot and normalized cell growth in soft agar of MCF-10A cells transduced with vector, SPCA2, GST, and membrane-anchored SPCA2 C terminus (GST-tagged); n = 3.

(E and F) Interaction between Orai1 N termini (N: aa 1–91), C termini (C: aa 255–301), intracellular loops (L1: aa 141–177), extracellular loops (L2: aa198-234), and SPCA2 full-length or N terminus.

(G) Interaction between Orai1 full-length and subregions of N terminus (N: aa 1–91; N1: aa 1–47; N2: aa 48–91), C terminus (C: aa 255–301), C terminus mutation (C-L273S), and SPCA2.

Error bars represent standard error (B) or standard deviation (A, C, and D).

Interestingly, C-terminal constructs of both SPCA isoforms, anchored to the membrane by a minimum of two transmembrane helices, were able to elicit Ca^{2+} influx and signaling. Consistent with this, critical amino acids within the C terminus were conserved in both isoforms from rat, mouse, and human. Therefore, we propose a mechanism in which accessibility of SPCA C termini is blocked in the full-length protein and binding of the N terminus to Orai1 is required for functional availability of the C terminus. Consistent with this hypothesis, we find that expression of the soluble N-terminal domain from SPCA2, but

not SPCA1, has a dominant-negative effect in blocking activation of Ca^{2+} signaling. Long-range conformational interactions between the N terminus and other cytosolic domains have been noted in SPCA and other P-type pumps, as well as changes in accessibility of the C-terminal tail (Huster and Lutsenko, 2003; Lecchi et al., 2005; Wei et al., 1999). Recently, Garside et al. (2010) identified an alternative transcript of SPCA2, encoding an ~20 kDa membrane-anchored C-terminal fragment, in tissues including brain, testes, salivary glands, and pancreas. Expression of this transcript was under the control of MIST1, a basic helix-loop-helix transcription factor, and appeared to be independent of the full-length transcript. This suggests the intriguing possibility that a C-terminal fragment of SPCA2 may elicit Ca^{2+} signaling independent of the full-length transporter.

Physiological and Pathophysiological Perspectives of SPCA2-Induced Ca^{2+} Signaling

The conventional role of ATP-powered Ca^{2+} pumps is to scavenge and extrude cytoplasmic Ca^{2+} in order to terminate a signal, and as a prerequisite for additional signaling events. Unexpectedly, high levels of expression of the Ca^{2+} efflux pump SPCA2 increased rather than lowered basal cytoplasmic Ca^{2+} levels, and conversely, attenuation of SPCA2 expression was accompanied by a decrease in basal Ca^{2+}. We speculate that this unconventional mechanism may be physiologically important in eliciting high rates of transcellular Ca^{2+} flux during lactation (Lee et al., 2006) and in other Ca^{2+}-secreting tissues, including salivary glands and intestinal epithelia, where SPCA2 is expressed at high levels. Total calcium concentration in milk can reach up to 100 mM, five to six orders of magnitude greater than typical cytoplasmic concentrations (~0.1 μM). Thus, there must be energy-dependent transport processes for effective transcellular movement of Ca^{2+} from blood into milk. In mammary gland, a 30-fold transcriptional increase in the plasma membrane Ca^{2+} pump isoform, PMCA2, is accompanied by apical efflux of Ca^{2+} into milk (Reinhardt et al., 2004). Compared to modest changes in SPCA1 levels, SPCA2 was found to be upregulated during pregnancy (~8-fold) and dramatically upon lactation (~35-fold on day 1). Furthermore, SPCA2 expression was restricted to the lumenal cells of lactating glands (Faddy et al., 2008). Our findings raise the possibility that SPCA2 traffics to the basolateral membrane where it can interact with Ca^{2+} channels to elicit Ca^{2+} influx and promote transcellular Ca^{2+} transport.

The unusual role of SPCA2 in activation of Ca^{2+} influx supersedes its ATP-dependent Ca^{2+} sequestering activity and may be a raison d'etre for its redundant expression along with SPCA1 in mammals and higher vertebrates. It is noteworthy that in lower eukaryotes (yeast, worm, fly) and vertebrates (fish) there is only a single ubiquitously expressed SPCA protein, which functions in transporting Ca^{2+} and Mn^{2+} into the secretory pathway. The advent of the SPCA2 gene in higher eukaryotes including frog, mouse, rat, and human may correlate with a newly required role in Ca^{2+} signaling. At the molecular level, a longer and divergent N terminus appears to have endowed SPCA2 with the ability to interact with unique partners, and discrete cell- and tissue-specific distribution would appear to regulate its function. Whereas in lactation, an exquisitely orchestrated developmental program ensures a coordinated regulation of Ca^{2+} pumps, channels, receptors, and buffers, there is emerging appreciation for a pronounced dysregulation of these processes in breast-derived tumor cells. For example, an aberrant switch in heterotrimeric G protein preference by the calcium sensing receptor, CaSR, in breast cancer cells leads to stimulation of cAMP signaling and increased secretion of PTHrP, which in turn is believed to contribute to a "vicious cycle" or feedforward loop of bone metastasis and osteolysis (Mamillapalli et al., 2008). Thus, the upregulation of SPCA2 in the altered signaling environment of tumor cells may result in constitutive Ca^{2+} signaling and cell growth. Inappropriate secretion of Ca^{2+} from these cells, in the absence of calcium buffers, could lead to microcalcifications that are diagnostic of breast cancer. Finally, the separation of signaling function from transport activity in SPCA2, evidenced by our findings, is highly unusual in pumps. An extreme case is SUR1, an ABC transporter that lacks known transport activity but is essential for conferring ATP sensitivity to K_{ATP} channels in insulin-secreting pancreatic β cells (Aittoniemi et al., 2009).

In summary, we identified a store-independent SPCA2-Orai1 signaling pathway. Upregulation of SPCA2 led to constitutively active Ca^{2+} signaling and correlated with oncogenic activity in breast cancer. Both SPCA2 and Orai1 emerge as druggable targets of therapeutic potential in the treatment of some breast cancer subtypes.

EXPERIMENTAL PROCEDURES

Materials and additional experimental procedures are described in the Supplemental Information.

SPCA2 Analysis in Human Breast Tumors

A gene expression dataset consisting of the microarray profiles of 295 primary human breast tumors (van de Vijver et al., 2002) was obtained from Rosetta Inpharmatics (Seattle, WA, USA). Tumors were assigned to transcriptional subtypes based on their gene expression profiles (Lumenal A [n = 88], Lumenal B [n = 81], Normal-like [n = 31], Basal-like [n = 46], and ERBB2+ [n = 49]) as described (Chang et al., 2005). One probe on the array (annotated as KIAA0703) corresponded to SPCA2. Tumors were grouped by transcriptional subtype and analyzed for SPCA2 expression. Statistical significance between groups was assessed by comparing medians using the Kruskall-Wallis test followed by Dunn's Multiple Comparison Test (Prism version 5, Graphpad Inc.).

NFAT Translocation Assay

Monitoring of nuclear translocation of NFAT was performed 24 hr post-transfection in HEK293 cells. Fresh medium was added 2 hr before the start of the experiment. Localization of NFAT-GFP and NFAT-mCherry in cells was examined by fluorescent microscopy. 100–300 cells were manually counted on each coverslip, 3 wells for each condition, and the fraction of cells with nuclear NFAT was calculated. Where indicated, 2 μM thapsigargin was added for 30 min, 10 μM miconazole was used for 1 hr, and 50 μM 2-APB was used for 1 hr.

Calcium Imaging and Mn^{2+} Quench

Cells were loaded with Fura-2 AM at 1 μg/ml in calcium recording buffer (126 mM NaCl, 2 mM $MgCl_2$, 4.5 mM KCl, 10 mM Glucose, 20 mM HEPES pH 7.4, 2 mM $CaCl_2$; no $CaCl_2$ was added for the 0 Ca^{2+} buffer) for 30 min at room temperature (RT). After loading, cells were rinsed in the same calcium recording buffer without Fura-2 for 20 min. Cells were excited at 340 nm and 380 nm, and Fura AM emission at 505 nm was monitored. Intracellular Ca^{2+} concentration was calculated based on the ratio of 340/380 nm. For Mn^{2+} quench of Fura-2 fluorescence, 0.5 mM of Mn^{2+} was added to nominally Ca^{2+}-free buffer. Cells were excited at 360 nm, the isosbestic point of

Fura-2, and emission at 505 nm was monitored. The average fluorescence of 10 time points (50 s) before Mn^{2+} addition was set as 100%.

Construction, Production, and Infection of Lentiviruses and Retroviruses

Replication-incompetent lentivirus was used to package shRNA for knockdown in MCF-7 cells and HEK293 cells. Cells were incubated with viruses for 48 hr and selected with puromycin (2-4 μg/ml).

Retroviral gene transfer and expression system (Clontech, Mountain View, CA, USA) was used for stable expression of SPCA2 in MCF-10 cells. SPCA2 gene was cloned into pLXRN vector to package retroviruses. Viruses were collected 48 hr after transfection and added to MCF-10A cells. Cells were treated with G418 (400 μg/ml) after 48 hr infection and selected cells were used to assay proliferation and colony formation in soft agar.

Cell Proliferation Assay

Proliferation was monitored using a Celltiter 96 Aqueous One Solution cell proliferation assay kit (Promega, Madison, WI, USA) according to manufacturer's instructions. Briefly, 0.5–1 × 10^4 cells were plated into a 96-well plate. After every 24 hr, 20 μl of Celltiter 96 Aqueous One Solution reagent was added to each well and incubated for 2 hr at 37°C, 5% CO_2. The absorbance at 490 nM was recorded using a 96-well plate reader.

Colony Formation in Soft Agar

Colony formation in soft agar assay was performed using a CytoSelect 96-well cell transformation assay kit (Cell Biolabs, San Diego, CA, USA). In a 96-well plate, 0.5–1 × 10^4 cells were resuspended in DMEM containing 0.4% agar and 10% FBS and layered onto a base agar consisting of DMEM with 0.6% agar and 10% FBS. Following solidification, growth medium was added on to the cell agar layer. One to two weeks later, colonies were imaged under the microscope, the agar layer was solubilized, and cells were lysed and quantified with CyQuant GR dye. The plate was read in a FLUOstar Optima plate reader (BMG Labtechnologies) using a 485/520 nm filter set.

Tumor Formation in Nude Mice

Female 4- to 6-week-old athymic nude mice (NCI) were received by the animal facility personnel and acclimated at the facility for 2 weeks. Estrogen pellets (SE-121, 0.72 mg/pellet, 60 days release) were obtained from Innovative Research of America. For each animal, a pellet was implanted into the back of the neck through a 1 cm cut and the wound was closed by a wound clip. After 3 days of implantation, the animals were ready to be injected with cells. MCF-7 cells transduced with control or SPCA2 shRNA or Orai1 shRNA were trypsinized and diluted to 1.5–3 × 10^7 cells per ml in PBS. 3 × 10^6 cells per animal were injected subcutaneously into the flank of each of 6–10 mice. The incidence of tumor formation was recorded in each animal once per week, starting 14–18 days after injection. Animal care was in accordance with institutional guidelines. One animal with subsequent tumor necrosis was euthanized, others were sacrificed after 10 weeks of observation.

Immunofluorescence

Cultured HEK293 and MCF-7 cells on coverslips were pre-extracted with PHEM buffer (60 mM PIPES, 25 mM HEPES, 10 mM EGTA, and 2 mM $MgCl_2$, pH 6.8) containing 0.025% saponin for 2 min, then washed twice for 2 min with PHEM buffer containing 0.025% saponin and 8% sucrose. The cells were fixed with a solution of 4% PFA and 8% sucrose in PBS for 30 min at room temperature and blocked with a solution of 1% BSA and 0.025% saponin in PBS for 1 hr. Primary antibodies were diluted 1:500 in 1% BSA and incubated with the cells for 1 hr. Alexa-Fluor 488 goat anti-rabbit IgG (Invitrogen) and Alexa-Fluor 568 goat anti-mouse IgG were used at a 1:1000 dilution for 30 min. Cells were mounted onto slides using Dako Fluorescent Mounting Medium. Slides were imaged on a Zeiss LSM510-Meta confocal microscope. In Figure 4A, anti-SPCA2 was used. In Figure 5H, anti-SPCA2, anti-SPCA1, and anti-HA were used to detect SPCA2N, SPCA1N, and HA-Orai1. In Figure S3C, anti-Myc, anti-SPCA1, and anti-Golgi97 were used to detect Myc-STIM1, HA-SPCA1, and Golgi 97. In Figure S5D, anti-SPCA2 and anti-HA were used to detect Myc-SPCA2 and HA-Orai1. In Figure S7B, anti-GST and anti-HA were used to detect GST-SPCA2C and HA-Orai1.

Coimmunoprecipitation and GST Pull-Down

Coimmunoprecipitation (co-IP) and GST pull-down assay in HEK293 cells were performed 24 hr after transfection. Co-IP in MCF-7 cells for endogenous proteins was performed 24–48 hr after seeding cells. Cells were lysed in lysis buffer (20 mM Tris-HCl, pH 7.4, 150 mM NaCl, 1 mM Na_3EDTA, 1 mM EGTA, 5 mM $Na_4P_2O_7$, 1 mM Na_3VO_4, 10 mM NaF, supplemented with 1% Triton X-100 and protease inhibitor cocktail [Roche]). 1/10 of the lysate was saved as "input." For co-IP, cell lysate was incubated 1 hr with GammaBind Plus Sepharose (GE Healthcare, Waukesha, WI, USA) for preclearance and 1–4 hr with antibodies (anti-Myc or anti-SPCA2) at 4°C. GammaBind beads were added and incubated for 1 hr at 4°C. For GST pull-down assay, cell lysate was incubated 2 hr with glutathione Sepharose 4B. Beads were washed using lysis buffer supplemented with 1% Triton X-100 before SDS-PAGE and immunoblotting. 1/2 of the "input" and 1/2 to 1/8 of the co-IP/pull-down fraction were loaded to SDS-PAGE gels. To co-IP cell-surface Orai1 with SPCA2, cells were biotin-labeled, lysed, and immunoprecipitated using anti-SPCA2 antibody. The proteins on the GammaBind beads were eluted with lysis buffer containing 1% SDS and incubated with neutravidin resin overnight at RT. Beads were washed in the same buffer. Only the portion of Orai1 that bound to SPCA2 at the cell surface was detected using SDS-PAGE and immunoblotting. 1/2 of the "input" and 1/2 of the biotinylated fraction were loaded to SDS-PAGE gels.

Functional Complementation in Yeast

Yeast growth assays were performed as described before (Xiang et al., 2005). The yeast strain K616 (*pmr1*Δ*pmc1*Δ*cnb1*Δ) was used as host for plasmids expressing SPCA2. Freshly grown cells were inoculated into each well of 96-well plates at 0.05 optical density (OD) 600 nm. Plates were incubated overnight at 30°C and resuspended by agitation, and $OD_{600\ nm}$ was measured using a FLUOstar Optima plate reader.

Three-Dimensional Structure Prediction

I-TASSER method was used to predict 3D protein structure from the primary amino acid sequence of the SPCA2 N terminus. I-TASSER was ranked as the No.1 server in recent CASP7 and CASP8 experiments (Critical Assessment of Protein Structure Prediction).

SUPPLEMENTAL INFORMATION

Supplemental Information includes Extended Experimental Procedures, seven figures, and one table and can be found with this article online at doi:10.1016/j.cell.2010.08.040.

ACKNOWLEDGMENTS

We thank Dr. Paul Worley and Dr. Guo Huang (Johns Hopkins University) for kind gifts of plasmids expressing Orai1, STIM1, and NFAT. This work was supported by grant GM62142 from the National Institution of Health to R.R., 569644 from the National Health and Medical Research and Cancer Council Queensland to G.R.M. and S.J.R.-T., Department of Defense-Center of Excellence Grant W81XWH-04-1-0595 to S.S., laboratory startup funds from the Albert Einstein College of Medicine to P.A.K., American Heart Association Pre-doctoral fellowship 0815058E to M.F., and American Psychological Association scholarship to H.M.F. and D.M.G.

Received: December 28, 2009
Revised: June 3, 2010
Accepted: August 24, 2010
Published: September 30, 2010

REFERENCES

Abdullaev, I.F., Bisaillon, J.M., Potier, M., Gonzalez, J.C., Motiani, R.K., and Trebak, M. (2008). Stim1 and Orai1 mediate CRAC currents and

store-operated calcium entry important for endothelial cell proliferation. Circ. Res. *103*, 1289–1299.

Aittoniemi, J., Fotinou, C., Craig, T.J., de Wet, H., Proks, P., and Ashcroft, F.M. (2009). Review. SUR1: a unique ATP-binding cassette protein that functions as an ion channel regulator. Philos. Trans. R. Soc. Lond. B Biol. Sci. *364*, 257–267.

Berridge, M.J., Bootman, M.D., and Roderick, H.L. (2003). Calcium signalling: dynamics, homeostasis and remodelling. Nat. Rev. Mol. Cell Biol. *4*, 517–529.

Bos, J.L. (1989). ras oncogenes in human cancer: a review. Cancer Res. *49*, 4682–4689.

Brandman, O., Liou, J., Park, W.S., and Meyer, T. (2007). STIM2 is a feedback regulator that stabilizes basal cytosolic and endoplasmic reticulum Ca^{2+} levels. Cell *131*, 1327–1339.

Cahalan, M.D., Zhang, S.L., Yeromin, A.V., Ohlsen, K., Roos, J., and Stauderman, K.A. (2007). Molecular basis of the CRAC channel. Cell Calcium *42*, 133–144.

Chang, H.Y., Nuyten, D.S., Sneddon, J.B., Hastie, T., Tibshirani, R., Sorlie, T., Dai, H., He, Y.D., van't Veer, L.J., Bartelink, H., et al. (2005). Robustness, scalability, and integration of a wound-response gene expression signature in predicting breast cancer survival. Proc. Natl. Acad. Sci. USA *102*, 3738–3743.

Clapham, D.E. (2007). Calcium signaling. Cell *131*, 1047–1058.

Clementi, E., and Meldolesi, J. (1996). Pharmacological and functional properties of voltage-independent Ca2+ channels. Cell Calcium *19*, 269–279.

Coleman, M.L., Marshall, C.J., and Olson, M.F. (2004). RAS and RHO GTPases in G1-phase cell-cycle regulation. Nat. Rev. Mol. Cell Biol. *5*, 355–366.

Cook, S.J., and Lockyer, P.J. (2006). Recent advances in Ca(2+)-dependent Ras regulation and cell proliferation. Cell Calcium *39*, 101–112.

Crabtree, G.R., and Olson, E.N. (2002). NFAT signaling: choreographing the social lives of cells. Cell Suppl. *109*, S67–S79.

Cullen, P.J., and Lockyer, P.J. (2002). Integration of calcium and Ras signalling. Nat. Rev. Mol. Cell Biol. *3*, 339–348.

Donovan, S., Shannon, K.M., and Bollag, G. (2002). GTPase activating proteins: critical regulators of intracellular signaling. Biochim. Biophys. Acta *1602*, 23–45.

Downward, J. (1996). Control of ras activation. Cancer Surv. *27*, 87–100.

Durr, G., Strayle, J., Plemper, R., Elbs, S., Klee, S.K., Catty, P., Wolf, D.H., and Rudolph, H.K. (1998). The medial-Golgi ion pump Pmr1 supplies the yeast secretory pathway with Ca2+ and Mn2+ required for glycosylation, sorting, and endoplasmic reticulum-associated protein degradation. Mol. Biol. Cell *9*, 1149–1162.

Faddy, H.M., Smart, C.E., Xu, R., Lee, G.Y., Kenny, P.A., Feng, M., Rao, R., Brown, M.A., Bissell, M.J., Roberts-Thomson, S.J., et al. (2008). Localization of plasma membrane and secretory calcium pumps in the mammary gland. Biochem. Biophys. Res. Commun. *369*, 977–981.

Fukasawa, K. (2007). Oncogenes and tumour suppressors take on centrosomes. Nat. Rev. Cancer *7*, 911–924.

Garside, V.C., Kowalik, A.S., Johnson, C.L., Direnzo, D., Konieczny, S.F., and Pin, C.L. (2010). Mist1 regulates the pancreatic acinar cell expression of ATP2C2, the gene encoding secretory pathway Ca2+-ATPase 2. Exp. Cell. Res., Published online June 23, 2010. 10.106/j.yexcr.2010.06.014.

Gwack, Y., Feske, S., Srikanth, S., Hogan, P.G., and Rao, A. (2007). Signalling to transcription: store-operated Ca2+ entry and NFAT activation in lymphocytes. Cell Calcium *42*, 145–156.

Hogan, P.G., Chen, L., Nardone, J., and Rao, A. (2003). Transcriptional regulation by calcium, calcineurin, and NFAT. Genes Dev. *17*, 2205–2232.

Huang, G.N., Zeng, W., Kim, J.Y., Yuan, J.P., Han, L., Muallem, S., and Worley, P.F. (2006). STIM1 carboxyl-terminus activates native SOC, I(crac) and TRPC1 channels. Nat. Cell Biol. *8*, 1003–1010.

Huster, D., and Lutsenko, S. (2003). The distinct roles of the N-terminal copper-binding sites in regulation of catalytic activity of the Wilson's disease protein. J. Biol. Chem. *278*, 32212–32218.

Lecchi, S., Allen, K.E., Pardo, J.P., Mason, A.B., and Slayman, C.W. (2005). Conformational changes of yeast plasma membrane H(+)-ATPase during activation by glucose: role of threonine-912 in the carboxy-terminal tail. Biochemistry *44*, 16624–16632.

Lee, W.J., Monteith, G.R., and Roberts-Thomson, S.J. (2006). Calcium transport and signaling in the mammary gland: targets for breast cancer. Biochim. Biophys. Acta *1765*, 235–255.

Lewis, R.S. (2007). The molecular choreography of a store-operated calcium channel. Nature *446*, 284–287.

Liou, J., Kim, M.L., Heo, W.D., Jones, J.T., Myers, J.W., Ferrell, J.E., Jr., and Meyer, T. (2005). STIM is a Ca2+ sensor essential for Ca2+-store-depletion-triggered Ca2+ influx. Curr. Biol. *15*, 1235–1241.

Mamillapalli, R., VanHouten, J., Zawalich, W., and Wysolmerski, J. (2008). Switching of G-protein usage by the calcium-sensing receptor reverses its effect on parathyroid hormone-related protein secretion in normal versus malignant breast cells. J. Biol. Chem. *283*, 24435–24447.

Matsumoto, Y., and Maller, J.L. (2002). Calcium, calmodulin, and CaMKII requirement for initiation of centrosome duplication in Xenopus egg extracts. Science *295*, 499–502.

Missiaen, L., Dode, L., Vanoevelen, J., Raeymaekers, L., and Wuytack, F. (2007). Calcium in the Golgi apparatus. Cell Calcium *41*, 405–416.

Monteith, G.R., McAndrew, D., Faddy, H.M., and Roberts-Thomson, S.J. (2007). Calcium and cancer: targeting Ca2+ transport. Nat. Rev. Cancer *7*, 519–530.

Morgan, M.P., Cooke, M.M., and McCarthy, G.M. (2005). Microcalcifications associated with breast cancer: an epiphenomenon or biologically significant feature of selected tumors? J. Mammary Gland Biol. Neoplasia *10*, 181–187.

Muik, M., Frischauf, I., Derler, I., Fahrner, M., Bergsmann, J., Eder, P., Schindl, R., Hesch, C., Polzinger, B., Fritsch, R., et al. (2008). Dynamic coupling of the putative coiled-coil domain of ORAI1 with STIM1 mediates ORAI1 channel activation. J. Biol. Chem. *283*, 8014–8022.

Oh-Hora, M., Yamashita, M., Hogan, P.G., Sharma, S., Lamperti, E., Chung, W., Prakriya, M., Feske, S., and Rao, A. (2008). Dual functions for the endoplasmic reticulum calcium sensors STIM1 and STIM2 in T cell activation and tolerance. Nat. Immunol. *9*, 432–443.

Parekh, A.B., and Putney, J.W., Jr. (2005). Store-operated calcium channels. Physiol. Rev. *85*, 757–810.

Park, C.Y., Hoover, P.J., Mullins, F.M., Bachhawat, P., Covington, E.D., Raunser, S., Walz, T., Garcia, K.C., Dolmetsch, R.E., and Lewis, R.S. (2009). STIM1 clusters and activates CRAC channels via direct binding of a cytosolic domain to Orai1. Cell *136*, 876–890.

Potier, M., Gonzalez, J.C., Motiani, R.K., Abdullaev, I.F., Bisaillon, J.M., Singer, H.A., and Trebak, M. (2009). Evidence for STIM1- and Orai1-dependent store-operated calcium influx through ICRAC in vascular smooth muscle cells: role in proliferation and migration. FASEB J. *23*, 2425–2437.

Reinhardt, T.A., Lippolis, J.D., Shull, G.E., and Horst, R.L. (2004). Null mutation in the gene encoding plasma membrane Ca2+-ATPase isoform 2 impairs calcium transport into milk. J. Biol. Chem. *279*, 42369–42373.

Roderick, H.L., and Cook, S.J. (2008). Ca2+ signalling checkpoints in cancer: remodelling Ca2+ for cancer cell proliferation and survival. Nat. Rev. Cancer *8*, 361–375.

Roos, J., DiGregorio, P.J., Yeromin, A.V., Ohlsen, K., Lioudyno, M., Zhang, S., Safrina, O., Kozak, J.A., Wagner, S.L., Cahalan, M.D., et al. (2005). STIM1, an essential and conserved component of store-operated Ca2+ channel function. J. Cell Biol. *169*, 435–445.

van de Vijver, M.J., He, Y.D., van't Veer, L.J., Dai, H., Hart, A.A., Voskuil, D.W., Schreiber, G.J., Peterse, J.L., Roberts, C., Marton, M.J., et al. (2002). A gene-expression signature as a predictor of survival in breast cancer. N. Engl. J. Med. *347*, 1999–2009.

Vanoevelen, J., Dode, L., Van Baelen, K., Fairclough, R.J., Missiaen, L., Raeymaekers, L., and Wuytack, F. (2005). The secretory pathway Ca2+/Mn2+-ATPase 2 is a Golgi-localized pump with high affinity for Ca2+ ions. J. Biol. Chem. *280*, 22800–22808.

Vig, M., and Kinet, J.P. (2007). The long and arduous road to CRAC. Cell Calcium *42*, 157–162.

Vig, M., Beck, A., Billingsley, J.M., Lis, A., Parvez, S., Peinelt, C., Koomoa, D.L., Soboloff, J., Gill, D.L., Fleig, A., et al. (2006). CRACM1 multimers form the ion-selective pore of the CRAC channel. Curr. Biol. *16*, 2073–2079.

Wei, Y., Marchi, V., Wang, R., and Rao, R. (1999). An N-terminal EF hand-like motif modulates ion transport by Pmr1, the yeast Golgi Ca(2+)/Mn(2+)-ATPase. Biochemistry *38*, 14534–14541.

Wei, Y., Chen, J., Rosas, G., Tompkins, D.A., Holt, P.A., and Rao, R. (2000). Phenotypic screening of mutations in Pmr1, the yeast secretory pathway Ca2+/Mn2+-ATPase, reveals residues critical for ion selectivity and transport. J. Biol. Chem. *275*, 23927–23932.

Wu, S., Skolnick, J., and Zhang, Y. (2007). Ab initio modeling of small proteins by iterative TASSER simulations. BMC Biol. *5*, 17.

Xiang, M., Mohamalawari, D., and Rao, R. (2005). A novel isoform of the secretory pathway Ca2+,Mn(2+)-ATPase, hSPCA2, has unusual properties and is expressed in the brain. J. Biol. Chem. *280*, 11608–11614.

Yang, S., Zhang, J.J., and Huang, X.Y. (2009). Orai1 and STIM1 are critical for breast tumor cell migration and metastasis. Cancer Cell *15*, 124–134.

Yeromin, A.V., Zhang, S.L., Jiang, W., Yu, Y., Safrina, O., and Cahalan, M.D. (2006). Molecular identification of the CRAC channel by altered ion selectivity in a mutant of Orai. Nature *443*, 226–229.